Zirconium coordination change upon the pressure-induced amorphization of cubic ZrW_2O_8 and $ZrMo_2O_8$

Tamas Varga* and Angus P. Wilkinson
School of Chemistry and Biochemistry, Georgia Institute of Technology, Atlanta, Georgia 30332-0400, USA
(Received 11 March 2009; published 30 June 2009)

Extended x-ray-absorption fine structure (EXAFS) and x-ray absorption near-edge structure (XANES) were used to examine cubic ZrW_2O_8 and cubic $ZrMo_2O_8$ that had been pressure amorphized at 7.5 and 5 GPa, respectively, in a multianvil press and recovered to ambient conditions. Data were taken at the W L_{III} and L_I or Mo *K* edges, as well as at the Zr *K* edge. They indicate an increase in the average coordination number of tungsten in ZrW_2O_8 and a less pronounced increase in that of molybdenum in $ZrMo_2O_8$, in agreement with previous work. Notably, the Zr *K*-edge XANES and EXAFS analyses provide strong evidence for a previously unreported change in the average Zr coordination from 6 to ~7 during the amorphization of both compounds.

DOI: 10.1103/PhysRevB.79.224119 PACS number(s): 61.50.Ks, 61.05.cj

I. INTRODUCTION

Pressure-induced amorphization (PIA) of the negative thermal-expansion (NTE) materials cubic ZrW_2O_8 (Refs. 1–8) and $ZrMo_2O_8$ (Refs. 8–10) has been quite widely studied. PIA occurs at relatively low pressures in these low-density materials. Cubic ZrW_2O_8, following a transition to its orthorhombic polymorph at lower pressure, was found to transform into an amorphous phase starting at 2.4 GPa with completion at <7.6 GPa.[5] $ZrMo_2O_8$ undergoes amorphization in the 1.7–4 GPa range.[10] Previously, we reported that amorphization is accompanied by an increase in the coordination number of tungsten and molybdenum in ZrW_2O_8 (Ref. 5) and $ZrMo_2O_8$,[10] respectively. This was less pronounced in the case of the molybdenum compound. It was concluded that the amorphous materials are probably metastable intermediates on a pathway to either high-pressure crystalline phases or decomposition products with higher metal coordination numbers than the starting phases. In their high-pressure simulation study on ZrW_2O_8, Pryde *et al.* argued that at high pressure, the ZrO_6 octahedra are more liable to distort than the WO_4 tetrahedra, and thus major coordination changes involving the zirconium were more likely than those involving tungsten.[11] Pereira *et al.* put forward a microscopic model for PIA, which involved the formation of new W-O bonds using the nonbridging oxygen atoms and freezing the structure of ZrW_2O_8 into a disordered state upon compression.[3,12] Later, from the reverse Monte Carlo modeling of total scattering data, Keen *et al.* confirmed that PIA in ZrW_2O_8 was accompanied by an increase in the tungsten coordination, while changes in zirconium coordination were not required.[7] Based on density functional theory (DFT) calculations for orthorhombic ZrW_2O_8, Figueirêdo *et al.* also suggested the formation of additional W-O bonds upon the amorphization of orthorhombic ZrW_2O_8.[6] In addition, they reported that the WO_x polyhedra are stiffer than ZrO_6 octahedra in orthorhombic ZrW_2O_8, as previously found for the cubic phase.[11] Recent interest in the microscopic mechanism of PIA for NTE materials along with the somewhat inconsistent results from the above simulation studies, specifically the anticipated softness of the ZrO_6 octahedra[6,11] versus the claim that changes in the zirconium coordination upon amorphization are not required,[7] prompted us to report the changes in zirconium coordination during the PIA of both ZrW_2O_8 and $ZrMo_2O_8$. X-ray absorption spectroscopy (XAS) measurements were performed at the zirconium *K* edge of amorphous ZrW_2O_8 and $ZrMo_2O_8$ samples that had been prepared at high pressure and recovered to ambient pressure. In addition, the local coordination environment around tungsten in ZrW_2O_8 and molybdenum in $ZrMo_2O_8$ were revisited using higher quality XAS data than that available from our prior *in situ* work.[5,10] In this paper, we report our findings regarding the evolution of the metal coordination environments upon PIA in the above compounds; we show that upon amorphization under our experimental conditions, the zirconium coordination increases from 6 to ~7 in both compounds. This, and a slight increase in molybdenum coordination for $ZrMo_2O_8$, and a more pronounced increase in tungsten coordination in ZrW_2O_8, is accompanied by a pronounced broadening of the distribution of close neighbor metal-metal distances. These findings are discussed in comparison to earlier results.

II. EXPERIMENTAL

Sample preparation. Cubic ZrW_2O_8—a stoichiometric amount of $ZrO(NO_3)_2 \cdot xH_2O$ (Aldrich, Milwaukee, WI) was thoroughly mixed and ground with 2 wt % excess of H_2WO_4 (Strem Chemicals, Newburyport, MA). The powder was heated at 1150 °C for 5, 24, and 36 h periods with intermittent ice-water quenching, drying (at 130 °C), and regrinding steps.

Amorphous ZrW_2O_8—cubic ZrW_2O_8 was compressed using a Walker-type high-pressure multianvil press at the Mineral Physics Institute, SUNY Stony Brook, NY. The pressure cell consisted of a platinum sample capsule in a 14 mm magnesia octahedron surrounded by eight 1 in. tungsten carbide cubes, all truncated on the corner facing the magnesia. Pyrophyllite and Teflon gaskets as well as balsa spacers were used between the cubes. ~140 mg cubic ZrW_2O_8 was placed into the Pt capsule and the sample was exposed to a pressure of about 7.5 GPa at room temperature for 2 h prior to slow decompression.

Cubic $ZrMo_2O_8$—$ZrMo_2O_7(OH)_2 \cdot 2H_2O$ was produced by the reaction of aqueous solutions of $ZrO(ClO_4)_2 \cdot 5H_2O$

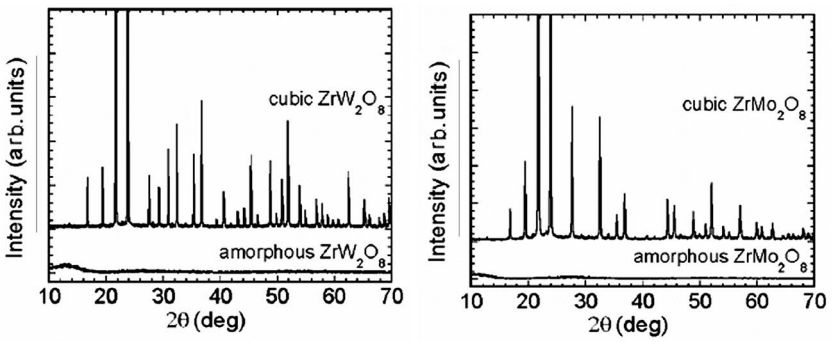

FIG. 1. Comparison of the x-ray diffraction patterns for the cubic and amorphous phases of ZrW_2O_8 and $ZrMo_2O_8$. No Bragg peaks appear in the pattern for the amorphous materials. Data collected using Cu $K\alpha$ radiation.

and $(NH_4)_6Mo_7O_{24}\cdot 4H_2O$ in acid medium by 3 days of refluxing. Then $ZrMo_2O_7(OH)_2\cdot 2H_2O$ was dehydrated by a series of low-temperature heat treatment steps (350 °C for 12 h, 375 °C for 15 min, 400 °C for 15 min, 425 °C for 30 min, and finally 450 °C for 30 min).

Amorphous $ZrMo_2O_8$—cubic $ZrMo_2O_8$ was compressed using the same Walker-type high-pressure multianvil press, and pressure cell assembly, as was employed for the preparation of amorphous ZrW_2O_8. ~100 mg cubic $ZrMo_2O_8$ was placed into the Pt capsule and the sample was exposed to a pressure of about 5 GPa at room temperature for 2 h prior to slow decompression.

Both amorphous samples were prepared at most a few weeks prior to the experiment (and their structure checked only a few days before the measurements, see Fig. 1) to minimize sample relaxation[5] after decompression. The Zr-containing reference phases ZrO_2 (Alfa Aesar, Ward Hill, MA) and $ZrSiO_4$ (Strem Chemicals, Newburyport, MA) were used as received. Preparation details of all other reference materials are given in the supplementary material.[13]

X-ray diffraction—all samples were characterized and their structure verified after synthesis (or purchase) by x-ray diffraction using a Scintag X1 diffractometer with a Peltier-cooled solid-state detector and a copper x-ray tube.

XAS data collection—all measurements were performed at beamline X11A of the NSLS, BNL, Upton, NY. Extended x-ray-absorption fine structure (EXAFS) and x-ray absorption near-edge structure (XANES) data were collected in transmission using a three-ion-chamber arrangement with a reference metal foil between the second and third detector. Samples of cubic and amorphous ZrW_2O_8, cubic and amorphous $ZrMo_2O_8$, and a series of reference compounds with different metal coordination were examined under ambient conditions. They were diluted and ground with boron nitride so that the maximum value of μt was ~1.5–2. XANES scans were performed around the W L_I edge (12.100 keV) using 25% monochromator detuning for harmonic rejection. EXAFS data were recorded at the W L_{III} edge (10.207 keV) with 30% detuning. XANES and EXAFS scans were performed around the Mo K edge (20.000 keV) using 10–15 % detuning. XANES and EXAFS data were recorded at the Zr K edge (17.998 keV) using 15% detuning. Data at each point were recorded for 2 s and, typically, three scans were performed with each sample.

Data processing and analysis—data processing was performed using the program ATHENA.[14,15] All fits to the EXAFS data were performed using the program ARTEMIS.[15,16] Further details of the XAS data collection and analysis can be found in the supplementary material.

III. RESULTS

Both previously amorphized samples were confirmed to be x-ray amorphous prior to the XAS experiments using laboratory XRD. X-ray diffraction patterns for the cubic and amorphous ZrW_2O_8 and $ZrMo_2O_8$ samples are shown in Fig. 1. No Bragg diffraction peaks were visible for any of the amorphous samples. Results from the W L_I-edge and Mo K-edge XANES are compared with those from our earlier *in situ* measurements[5,10] in the supplementary material.

W L_{III}-edge and Mo K-edge EXAFS—the Fourier-transformed $k\chi(k)$ (FT magnitude) curves of the cubic and amorphous materials are compared with one another in Figs. 2 and 3. There is clearly a change in the spectrum of amorphous ZrW_2O_8 when compared to the cubic material (Fig. 2); the back-scattering magnitudes are reduced with a more dramatic suppression at greater interatomic distances. A similar change is visible for $ZrMo_2O_8$ but it is apparently less significant (Fig. 3). Further discussion of these W L_{III}-edge and Mo K-edge EXAFS data is presented, along with a comparison to our earlier *in situ* results,[5,10] in the supplementary material.

Zr K-edge XANES and EXAFS—the XANES indicate a change in Zr coordination on amorphization for both ZrW_2O_8 and $ZrMo_2O_8$ (see Fig. 4). XANES spectroscopy at the Zr K edge has been used before for qualitative comparison of species with different Zr-coordination environments.[17,18] By visual examination of the absorption edges, an average coordination of ~7 could be estimated in both amorphous materials based on the great resemblance of their edge features to that of ZrO_2, which contains Zr in 7 coordination.[19] The difference among 6 (cubic ZrW_2O_8 and $ZrMo_2O_8$), 7 (ZrO_2), and 8 ($ZrSiO_4$) (Ref. 20) coordinations is clearly distinguishable.

The Fourier-transformed $k\chi(k)$ curves obtained from the Zr K-edge EXAFS data obtained for model compounds ZrO_2 and $ZrSiO_4$, and for cubic and amorphous ZrW_2O_8 and $ZrMo_2O_8$ are shown and discussed in the supplementary material.

In Table I, we present our estimates of the average Zr-O bond lengths derived by fitting the room-temperature Zr K-edge EXAFS data for cubic and amorphous ZrW_2O_8 and $ZrMo_2O_8$, respectively, along with values for two reference compounds with 7 (ZrO_2) and 8 ($ZrSiO_4$) coordina-

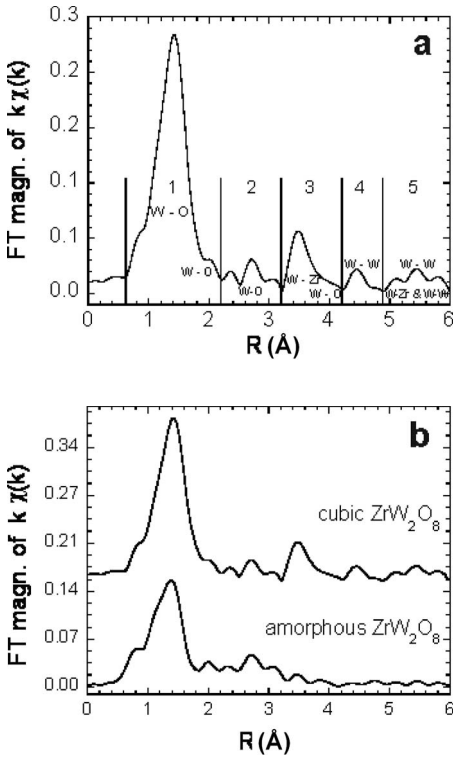

FIG. 2. (a) Contribution of the different metal-oxygen and metal-metal SS and MS paths to the Fourier-transformed *R*-space spectrum of cubic ZrW_2O_8. (b) FT magnitude curves for cubic and amorphous ZrW_2O_8.

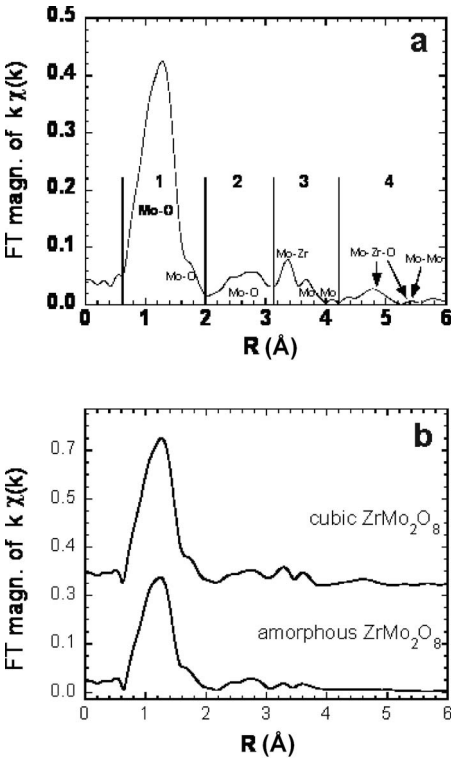

FIG. 3. (a) Contribution of the different metal-oxygen and metal-metal SS and MS paths to the Fourier-transformed *R*-space spectrum of cubic $ZrMo_2O_8$. (b) FT magnitude curves for cubic and amorphous $ZrMo_2O_8$.

tions. The average metal-oxygen distance has been used as a metric by other workers when looking at changes in coordination on compression.[21,22] In general, the average metal-oxygen bond length for a coordination polyhedron increases as the coordination number of the metal increases, and this variation is large enough for us to use the estimated average Zr-O distance from our EXAFS analysis as an indicator of the coordination number for zirconium. Note, in the absence of a change in coordination number, the average Zr-O distance would be expected to decrease on compression. Details of the EXAFS analysis can be found in the supplementary material. The average Zr-O distance derived for our crystalline samples increases with increasing coordination number as expected. As the average Zr-O distance for both amorphous materials is significantly larger than that for the starting crystalline materials and close to the value obtained for ZrO_2, we believe that the average Zr coordination in ZrW_2O_8 and $ZrMo_2O_8$ changed from 6 to around 7 as the compounds amorphized on compression. This conclusion is fully consistent with the XANES measurements (Fig. 4).

IV. DISCUSSION

Our findings based on the W L_I-edge and Mo *K*-edge XANES are in agreement with those previously reported based on *ex situ* and *in situ* studies of ZrW_2O_8 and $ZrMo_2O_8$.[5,10] Both the EXAFS and XANES revealed an increase in the average coordination number of tungsten in ZrW_2O_8 and a marginal change in molybdenum coordination away from tetrahedral in $ZrMo_2O_8$ (see supplementary material).

The local structure of cubic ZrW_2O_8 has already been studied in detail by XAS.[23,24] This information was used to help identify the contributions of different scattering paths to the EXAFS Fourier-transform magnitudes for cubic and amorphous ZrW_2O_8 and $ZrMo_2O_8$ (Figs. 2 and 3, respec-

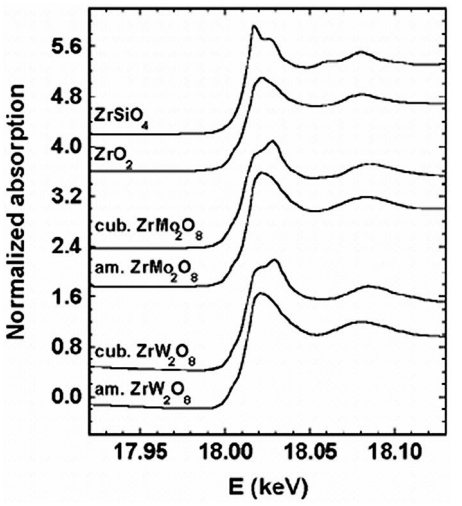

FIG. 4. Zr *K*-edge XANES spectra for cubic and amorphous ZrW_2O_8 and $ZrMo_2O_8$ containing 6 coordinate Zr along with two reference compounds with 7 (ZrO_2) and 8 ($ZrSiO_4$) Zr coordination.

TABLE I. First-shell average Zr-O bond lengths obtained from room-temperature EXAFS data for cubic and amorphous ZrW_2O_8 and $ZrMo_2O_8$, respectively, along with two reference compounds with 7 (ZrO_2) and 8 ($ZrSiO_4$) coordinations. The fits were carried out in Fourier-filtered k space using only one scattering path (k range: 2.9–15 $Å^{-1}$; R range: 0.90–2.25 Å). Bond lengths were calculated for multiplicities (number of O around the central atom, Zr) of 6 and 8.

	Average Zr-O bond length (Å)	
Sample	6 coordinate	8 coordinate
Cubic ZrW_2O_8 (tetrahedral)	2.056(8)	2.057(7)
Cubic $ZrMo_2O_8$ (tetrahedral)	2.063(6)	2.065(6)
Amorphous ZrW_2O_8	2.092(8)	2.094(7)
Amorphous $ZrMo_2O_8$	2.090(9)	2.092(7)
ZrO_2 (7 coordinate)	2.100(8)	2.101(8)
$ZrSiO_4$ (8 coordinate)	2.140(9)	2.142(9)

tively). In the supplementary material we provide a detailed discussion of the local structure of cubic ZrW_2O_8 and $ZrMo_2O_8$ as seen by EXAFS, and we tabulate the results from out fits for all the tungsten and molybdenum containing compounds. Here, only a graphical illustration of the contribution of the different metal-oxygen and metal-metal single-scattering (SS) and multiple-scattering (MS) paths to the Fourier-transformed R-space spectrum of cubic ZrW_2O_8 and $ZrMo_2O_8$ is given in Figs. 2(a) and 3(a), respectively. Figures 2(b) and 3(b) reveal the following qualitative changes in $k\chi(k)$ upon amorphization: (i) all the peak amplitudes are reduced in the amorphous material relative to the cubic one, (ii) this reduction is most significant for the metal-metal correlations, that is, those associated with either W-Zr, Mo-Zr, W-W, or Mo-Mo scattering paths (they may include oxygen, e.g., Mo-Zr-O), (iii) the backscattering associated with interatomic distances above 4 Å seems to be washed out completely on amorphization. This suggests that the distribution of the metal-metal distances becomes quite large upon the loss of long-range order, while the distribution of nearest-neighbor metal-oxygen distances remains small, as quite well-defined coordination polyhedra persist in the amorphous phase. The loss of well-defined features above 4 Å interatomic distances [Figs. 2(b) and 3(b)] is in agreement with the almost featureless pair distribution functions for $r > 4$ Å for amorphous ZrW_2O_8 reported by Keen *et al.*[7]

In the remainder of this discussion, we will focus on our findings from the Zr K-edge XAS. According to the report of Keen *et al.*, for a sample recovered from ~4 GPa, there is no clear evidence for a change in zirconium coordination at this pressure.[7] In their report, they consider two different models for the structure of amorphous ZrW_2O_8: one involving possible bond formation between nonbridging oxygen atoms and a nearby Zr atom giving rise to new Zr-O-W linkages [model A (Ref. 7)], and model B, which involves the formation of additional W-O-W linkages rather than Zr-O-W, while Zr retains sixfold coordination. They claim model B to be the operating mechanism, as it gave better agreement with their data.

Our Zr K-edge XANES data revealed that the average Zr coordination increases from 6 to approximately 7 on amorphization, both in ZrW_2O_8 and $ZrMo_2O_8$, indicating that distortion of the ZrO_6 octahedra is significant after recovery from 7.5 GPa for ZrW_2O_8 and 5 GPa for $ZrMo_2O_8$. Our results are consistent with an amorphization mechanism involving possible bond formation between nonbridging oxygen atoms and a nearby Zr atom (model A by Keen *et al.*[7]).

Unfortunately, due to the lack of either *in situ* Zr K-edge data at various pressures or the corresponding *ex situ* data for phases recovered from different pressures below 7.5 GPa, we do not know whether the changes in zirconium coordination that we observe occurred on initial amorphization or at higher pressure. Here, we note that the possible dependence of the amorphous material's structure on the pressure used for the amorphization should also be remembered when comparing the amorphization of ZrW_2O_8 and $ZrMo_2O_8$ using Mo/W XAS. Coordination numbers tend to increase with pressure; thus the lower pressure in the work of Keen *et al.*[7] may explain the difference between the tungsten coordination suggested by our EXAFS measurements (distorted 6 coordinate), and by model A of Keen *et al.* (mix of 4 and 5 coordinate tungstens). Other workers used higher pressure in their studies of the amorphization of ZrW_2O_8. For example, Catafesta *et al.*,[12] and Figueiredo *et al.*[6] studied samples recovered from 7.7 GPa. Although, these groups also favor an amorphization mechanism involving the formation of additional W-O bonds, their data are not inconsistent with an increase in Zr coordination due to additional Zr-O bond formation. Thus, our results are not inconsistent with previous reports but point to the possible importance of a previously unobserved change in Zr coordination during amorphization or at higher pressures after amorphization.[6,12]

The Mo K-edge XANES and EXAFS demonstrate that the pressure-induced amorphization of cubic $ZrMo_2O_8$ at ~5 GPa is not accompanied by any dramatic changes in the molybdenum coordination on amorphization. The reduction in the FT magnitude associated with metal-metal scattering paths was smaller than in amorphous ZrW_2O_8. The Zr K-edge data indicated a change in Zr coordination similar to that seen for ZrW_2O_8. The pressures employed by us to amorphize cubic $ZrMo_2O_8$ (5 GPa) and ZrW_2O_8 (7.5 GPa) were chosen to be above the reported amorphization pressure ranges for both $ZrMo_2O_8$ [1.7–4.1 GPa (Ref. 10)], and ZrW_2O_8 [2.3–7.6 GPa (Ref. 5)]. As the onset of amorphization is at lower pressure for the molybdate, the pressure used for our amorphization experiment was also lower. It is possible that higher Mo coordination can be achieved in amorphous $ZrMo_2O_8$ at pressures above 5 GPa, while this pressure was sufficient to change the Zr coordination.

From the W L_{III}-edge EXAFS (Fig. 2), it was not clear whether the W-Zr or the W-W scattering is more important among the metal-metal correlations in the amorphous material. The Zr K-edge EXAFS provided a useful insight into this question. As practically no contribution from metal-metal scattering paths was needed to adequately fit the Zr K-edge EXAFS data for amorphous ZrW_2O_8 (see Fig. S14 in the supplementary material[13]), we believe that the primary metal-metal contribution to the W EXAFS is W-W (single and multiple paths), and not Zr-W. This suggests that the distribution of Zr-W distances is larger in the disordered material than the distribution of W-W distances. In the

Zr *K*-edge EXAFS for amorphous $ZrMo_2O_8$ (also in the supplementary material,[13] Fig. S15) the Zr-Mo nearest-neighbor backscattering was not negligible. This suggests a narrower distribution of Zr-*X* (*X*=Mo or W) distances in the $ZrMo_2O_8$ recovered from ~5 GPa than in amorphous ZrW_2O_8 recovered from 7.5 GPa.

Regarding the general picture of what drives pressure-induced amorphization in these compounds, distortion of the ZrO_6 octahedra, as indicated by the Zr *K*-edge XAS further supports the invalidity of a simple polyhedral tilting model for amorphization.[5,10] The increase in the coordination number of Zr from 6 to ~7 does not exclude a kinetically frustrated decomposition as the amorphization mechanism, given that the Zr in ZrO_2 is 7 coordinated.[19] This is true for both ZrW_2O_8 and $ZrMo_2O_8$. However, the increased Zr coordination is inconsistent with amorphous ZrW_2O_8 being an intermediate on a pathway to the known high-pressure crystalline form of ZrW_2O_8 with a α-U_3O_8 related structure, as this material contains sixfold-coordinated Zr atoms.[25] To our knowledge, no high-pressure phase with fivefold or sixfold Mo, and sevenfold Zr coordination has been reported for $ZrMo_2O_8$, although a monoclinic form of $ZrMo_2O_8$ with 8 coordinate zirconium and 5 coordinate molybdenum is known.[9]

V. CONCLUSIONS

Zr *K*-edge XAS experiments revealed a previously unidentified increase in zirconium coordination number in amorphous ZrW_2O_8 and $ZrMo_2O_8$ prepared at high pressure. Our observations are not contrary to prior *in situ* or *ex situ* measurements[5,10] but suggest a different aspect to the amorphization of these materials; the formation of additional Zr-O-W or Zr-O-Mo links. The atomic-scale PIA mechanisms for cubic ZrW_2O_8 and $ZrMo_2O_8$ are somewhat different from one another, in agreement with earlier work.[5,10] While the pressure-induced amorphization of ZrW_2O_8 is accompanied by a significant increase in the average tungsten coordination, the average molybdenum coordination in $ZrMo_2O_8$ changes to a small extent on amorphization.

ACKNOWLEDGMENTS

A.P.W. is grateful for support from National Science Foundation under Grants No. DMR-0203342 and No. DMR-0605671. We acknowledge the Mineral Physics Institute of SUNY Stony Brook for providing access to the high-pressure apparatus and technical support. Use of the National Synchrotron Light Source, Brookhaven National Laboratory, was supported by the U.S. Department of Energy, Office of Science, Office of Basic Energy Sciences under Contract No. DE-AC02-98CH10886. We would like to thank Bruce Ravel for his help with setting up the XAS experiment. We also thank Mehmet Cetinkol for his help with the data collection.

*Author to whom correspondence should be addressed. Present address: Environmental and Molecular Sciences Laboratory, Pacific Northwest National Laboratory, Richland, WA 99352; tamas.varga@pnl.gov

[1] C. A. Perottoni and J. A. H. de Jornada, Science **280**, 886 (1998).
[2] T. R. Ravindran, A. K. Arora, and T. A. Mary, J. Phys.: Condens. Matter **13**, 11573 (2001).
[3] A. S. Pereira, C. A. Perottoni, and J. A. H. de Jornada, J. Raman Spectrosc. **34**, 578 (2003).
[4] C. A. Perottoni, J. E. Zorzi, and J. A. H. da Jornada, Solid State Commun. **134**, 319 (2005).
[5] T. Varga, A. P. Wilkinson, A. C. Jupe, C. Lind, W. A. Bassett, and C.-S. Zha, Phys. Rev. B **72**, 024117 (2005).
[6] C. A. Figueirêdo, J. Catafesta, J. E. Zorzi, L. Salvador, I. J. R. Baumvol, M. R. Gallas, J. A. H. da Jornada, and C. A. Perottoni, Phys. Rev. B **76**, 184201 (2007).
[7] David A. Keen, Andrew L. Goodwin, Matthew G. Tucker, Martin T. Dove, John S. O. Evans, Wilson A. Crichton, and Michela Brunelli, Phys. Rev. Lett. **98**, 225501 (2007).
[8] T. Varga, C. Lind, A. P. Wilkinson, H. Xu, C. E. Lesher, and A. Navrotsky, Chem. Mater. **19**, 468 (2007).
[9] A. Grzechnik and W. A. Crichton, Solid State Sci. **4**, 1137 (2002).
[10] T. Varga, A. P. Wilkinson, C. Lind, W. A. Bassett, and C.-S. Zha, Solid State Commun. **135**, 739 (2005).
[11] A. K. A. Pryde, M. T. Dove, and V. Heine, J. Phys.: Condens. Matter **10**, 8417 (1998).
[12] J. Catafesta, J. E. Zorzi, C. A. Perottoni, M. R. Gallas, and J. A. H. da Jornada, J. Am. Ceram. Soc. **89**, 2341 (2006).
[13] See EPAPS Document No. E-PRBMDO-79-069922 for details on the preparation of the reference materials, and a detailed discussion of W L_I- and Mo *K*-edge XANES, and W L_{III}- and Mo *K*-edge EXAFS data and fitting, as well as the local structure of cubic ZrW_2O_8 and $ZrMo_2O_8$. For more information on EPAPS, see http://www.aip.org/pubservs/epaps.html.
[14] B. Ravel, computer code ATHENA, Washington, D.C., 2001–2003.
[15] M. Newville, J. Synchrotron Radiat. **8**, 322 (2001).
[16] B. Ravel, computer code ARTEMIS, Washington, D.C., 2001–2003.
[17] G. Mountjoy, R. Anderson, R. J. Newport, and M. E. Smith, J. Phys.: Condens. Matter **12**, 3505 (2000).
[18] H. Kanai, Y. Okumura, K. Utani, K. Hamada, and S. Imamura, Catal. Lett. **76**, 207 (2001).
[19] D. K. Smith and H. W. Newkirk, Acta Crystallogr. **18**, 983 (1965).
[20] R. M. Hazen and L. W. Finger, Am. Mineral. **64**, 196 (1979).
[21] C. Meade, R. J. Hemley, and H. K. Mao, Phys. Rev. Lett. **69**, 1387 (1992).
[22] J. P. Itie, A. Polian, G. Calas, J. Petiau, A. Fontaine, and H. Tolentino, Phys. Rev. Lett. **63**, 398 (1989).
[23] D. Cao, F. Bridges, G. R. Kowach, and A. P. Ramirez, Phys. Rev. Lett. **89**, 215902 (2002).
[24] D. Cao, F. Bridges, G. R. Kowach, and A. P. Ramirez, Phys. Rev. B **68**, 014303 (2003).
[25] A. Grzechnik, W. A. Crichton, K. Syassen, P. Adler, and M. Mezouar, Chem. Mater. **13**, 4255 (2001).